Mass transfer at the surface in LES of wind-driven shallow water flow with Langmuir circulation

Andrés E. Tejada-Martínez[1], Cigdem Akan[1] and Chester E. Grosch[2]

[1] *University of South Florida, Tampa, FL, USA, E-mail: aetejada@usf.edu*
[2] *Ocean, Earth and Atmospheric Sciences & Center for Coastal Physical Oceanography, Old Dominion University, Norfolk, VA, USA, E-mail: enright@ccpo.odu.edu*

Abstract. Surface mass (scalar) transfer results from large-eddy simulation (LES) of wind-driven shallow water flow with and without full-depth Langmuir circulation (LC) are reported. Our work is motivated by the airborne infrared imagery of Marmorino *et al*. (2005) suggesting that LC can affect mass transfer through stretching and compression of molecular sublayers below the surface (i. e. below the air-water interface). LC also serves as an effective mechanism for sea surface renewal of low concentration fluid. LES guided by the full-depth LC measurements of Gargett *et al*. (2004), shows that this large-scale, downwindelongated structure increases surface mass transfer velocity (a measure of mass transfer efficiency) by approximately 60 percent with respect to a similar flow without surface wave effects (i.e. without LC). Statistical analysis of LES variables reveals that full-depth LC dominates near-surface mass transport as well as transport everywhere else in the water column. In the absence of LC, nearsurface small eddies contribute towards the mass transport at the air-water interface. Finally, the LES is used to test the accuracy of surface renewal-based parameterizations (models) in predicting surface transfer velocity in flows with full-depth LC. It is found that the transfer velocity parameterization of Gulliver and Halverson (1989) based on surface renewal time scale given by characteristics of large-scale (full-depth) streamwise vortices performs best compared to parameterizations based on turbulent quantities measured at the surface.

Key Words: large-eddy simulation, full-depth Langmuir circulation, surface mass transfer

1. Introduction

For sparingly soluble gases such as CO_2, near-surface oceanic turbulence greatly influences gas transfer rates across the air-sea interface. This is due to the fact that the diffusivity of sparingly soluble gases in air is much larger than in water (Donelan and Wanninkof 2000).

The water-side gas concentration diffusion boundary layer is embedded within the thermal boundary layer (often referred to as the cool skin) and both are

embedded within the viscous sublayer. A number of parameterizations capable of describing bulk characteristics of thermal and diffusion sublayers (such as surface gas transfer velocity and temperature difference across the cool skin) have emerged. Among these parameterizations are those derived from surface renewal theory (e.g. Liu and Businger (1975), Liu *et al*. (1979), Soloviev and Schlüssel (1994)). Surface renewal theory is based on an intermittent renewal of the cool, high gas concentration water at the surface with warm, low gas concentration water from below. A number of hydrodynamic processes are taken to influence this periodic renewal of surface water. Under calm conditions, thermal convection is prominent in determining surface renewal. For moderate wind conditions (characterized by wind speeds between 5 and 10 m s^{-1}), surface renewal is influenced by microscale wave breaking, specifically viscous wind-stress variations caused by the rollers on microbreakers (Csanady, 1990; Soloviev and Schlüssel, 1994). For high wind conditions (characterized by wind speeds greater than 10 m s^{-1}), surface renewal is strongly dominated by long surface wave breaking.

A turbulent process often neglected in parameterizations of surface mass transfer is wave-current interaction generating Langmuir circulation (LC) under low to high wind speeds. LC influences surface mass transport through stretching and compression of the air-water interface (Marmorino *et al*. 2005) thereby disrupting surface molecular sublayers. Furthermore, the enhanced mixing caused by LC presents a strong mechanism for surface renewal. LC consist of pairs of parallel counter-rotating vortices (or cells) oriented approximately in the downwind direction. These cells are characteristic of the turbulence (i.e. the Langmuir turbulence) advected by the mean flow. The surface convergence of each Langmuir cell generates a downwelling region (or limb) characterized by negative vertical velocity fluctuations while the bottom divergence generates an upwelling region characterized by positive vertical velocity fluctuations, leading to increased levels of mixing. Originally described by Langmuir (1938), LC is now generally accepted to be the result of wave-current interaction or, more specifically, the interaction between the wind-driven shear current and the Stokes drift current induced by surface gravity waves. Thorpe (2004) reviewed the numerous field observations and computations of LC that have been made over the last few decades. Most of these works have dealt with LC within the upper ocean mixed layer constrained below by a thermocline. Recent observations of Gargett *et al*. (2004) and Gargett and Wells (2007) have led to the discovery of LC extending throughout the entire water column. These observations were made on the shallow shelf coastal region of southern New Jersey in a 15 m-deep water column undergoing moderate to strong wind and wave forcing. Typical wind speeds were between 7 m s^{-1} and 11 m s^{-1}, wave amplitudes were approximately 1 m, and

wave periods were approximately 8 seconds. These full-depth Langmuir cells, reaching the bottom boundary layer, have been termed supercells because of their strong influence on sediment resuspension and transport.

Infrared observations of Marmorino *et al*. (2005) led to the discovery of similar shallow water Langmuir cells off the West Florida coast near the mouth of Tampa Bay under moderate wind conditions (4.2 m s^{-1} to 5.5 m s^{-1}). The impact of the cells on the ocean cool skin was clearly distinguishable in their infrared images. Surface divergence zones of the Langmuir cells induced a horizontal stretching and thus a thinning of the cool skin resulting in a slight increase in surface temperature in order to match the surface heat flux. On the other hand, surface converge zones induced a compression and thus a thickening of the cool skin resulting in a slight decrease in surface temperature. Along the surface convergence of the cells, the surface temperature was about 0.2 ºC cooler than the surrounding surface water.

Tejada-Martínez and Grosch (2007) and Tejada-Martínez *et al*. (2009) performed laboratory-scale LES of a finite-depth, wind-driven shear current with full-depth LC guided by the field measurements of Gargett *et al*. (2004) and Gargett and Wells (2007). The LES was at a lower Reynolds number than the field measurements, but was driven by the same wave forcing relative to wind forcing measured by Gargett and collaborators in the field. LES was performed at a lower Reynolds number in order to resolve the bottom viscous sublayer and undertand its behavior under the influence of the full-depth LC. Predictions from the LES compared favorably with in-water measurements. For example, Tejada-Martínez *et al*. (2009) show LES-computed velocity fluctuations dimensionalized with the wind stress friction velocity measured during the field observations of Gargett *et al*. 2004 and Gargett and Wells 2007. The magnitude of the LES fluctuations was in good agreement with those of the field measurements during episodes of LC, which shows that the computed laboratory-scale (low-Reynolds number) LC flow is able to scale-up to field-scale LC flows. Furthermore, the structure of the Langmuir cells, manifested as a secondary turbulent structure in the shear flow, was consistent with that measured during the in-water observations.

We extend the LES of full-depth LC of Tejada-Martínez and Grosch (2007) in order to understand the impact of the Langmuir cells on near-surface scalar transport. The LES resolves the surface molecular sublayers for momentum and diffusion, thus mass transfer velocity is explicitly computed without resorting to parameterizations. LES with molecular sublayer resolution presents a framework in which parameterizations of transfer velocity may be validated via comparison with transfer velocity obtained directly in the LES.

2. LES equations

The governing dimensionless, low-pass spatially filtered and time filtered equations augmented by the Craik-Leibovich vortex force accounting for LC (McWilliams *et al*. 1997) are

$$\begin{aligned} \frac{\partial \overline{u}_i}{\partial x_i} &= 0 \\ \frac{\partial \overline{u}_i}{\partial t} + \overline{u}_j \frac{\partial \overline{u}_i}{\partial x_j} &= -\frac{\partial \overline{\Pi}}{\partial x_i} + \frac{1}{Re}\frac{\partial^2 \overline{u}_i}{\partial x_j^2} + \frac{\partial \tau_{ij}}{\partial x_j} + \frac{1}{La_t^2}\varepsilon_{ijk}\phi_j^s \overline{\omega}_k \\ \frac{\partial \overline{C}}{\partial t} + \overline{u}_j \frac{\partial \overline{C}}{\partial x_j} + \frac{1}{La_t^2}\phi_j^s \frac{\partial \overline{C}}{\partial x_j} &= \frac{1}{ReSc}\frac{\partial^2 \overline{C}}{\partial x_j^2} + \frac{\partial q_j}{\partial x_j} \end{aligned} \tag{1}$$

where ε_{ijk} is the totally antisymmetric third rank tensor, an over-bar denotes application of the low-pass spatial and temporal filters and $\overline{u}_i$ and $\overline{\omega}_i$ are the i-th components of the dimensionless space and time filtered velocity and vorticity, respectively, in the Cartesian coordinate system (x_1, x_2, x_3) depicted in Figure 1. The space and time filtered pressure and scalar concentration are denoted as $\overline{\Pi}$and $\overline{C}$, respectively.

The fourth (last) term on the right hand side of the second equation in (1) is the non-dimensionalized Craik-Leibovich vortex force defined as the Stokes drift velocity crossed with the filtered vorticity. Time filtering filters out surface gravity waves and the Craik-Leibovich vortex force accounts for the effect of these waves on the flow, giving rise to Langmuir circulation (LC). The dimensionless Stokes drift velocity is defined following Phillips (1967) as

$$\phi_1^s = \frac{\cos h(2(\kappa x_3 + 1))}{2 \sin h^2(2\kappa)} \quad \text{and} \quad \phi_2^s = \phi_3^s = 0\,, \tag{2}$$

where κ is the dimensionless dominant wavenumber of the filtered-out surface gravity waves and can be obtained from their dominant wavelength.

The characteristic flow velocity is taken as bottom friction velocity, u_τ, where $u_\tau = (\tau_{wall}/\rho_o)^{1/2}$, τ_{wall} is the mean viscous shear stress at the no-slip bottom boundary or wall of the flow domain (as depicted in Figure 1) and ρ_o is the constant density. In our LES of wind-driven flows, the computed τ_{wall} is equal to the wind stress applied at the surface (see Figure 1b). In our pressure gradient-driven flows, the prescribed driving body force is balanced by the force at the wall exerted by τ_{wall} (see Figure 1a). Non-dimensionalizing the governing equations with characteristic flow velocity u_τ and characteristic length scale δ (domain half-depth) gives rise to

the Reynolds number $Re=u_\tau\ \delta/\nu$ (with ν the kinematic viscosity) and the turbulent Langmuir number, $La_t=(u_*/u_s)^{1/2}$, both appearing in (1). In the definition of La_t, the characteristic Stokes drift velocity is $u_s=\omega k a^2$, where ω is the dominant frequency, k is the dominant wavenumber and a is the amplitude of the surface gravity waves. Note that La_t^2 is inversely proportional to wave forcing relative to wind forcing. Although not shown here, also note that the Stokes drift velocity serves to modify the pressure giving rise to $\overline{\Pi}$ as defined by McWilliams *et al*. (1997). The Schmidt number in the scalar equation in (1) is defined as $Sc=\nu/D_c$ where D_c is the molecular diffusivity of the scalar.

The subgrid-scale (SGS) stress τ_{ij} and the SGS scalar flux q_{ij} in (1), generated by spatial filtering of the governing equations, are modeled using the dynamic Smagorinsky model

$$\tau_{ij}=2\underbrace{(C_s\Delta)^2|\overline{S}|}_{\text{eddy viscosity}}\overline{S}_{ij}, \quad \text{and} \quad q_j=\underbrace{(C_s\Delta)^2|\overline{S}|}_{\text{eddy diffusivity}}\frac{\partial\overline{C}}{\partial x_j} \tag{3}$$

where Δ is the width of the spatial filter (i.e. implicitly set by the smallest characteristic length scale resolved by the LES), C_s is the Smagorinsky coefficient, C_c is an analogous coefficient for the SGS scalar flux, $\overline{S}_{ij}=(\overline{u}_{i,j}+\overline{u}_{j,i})/2$ is the filtered strain-rate tensor, and $|\overline{S}|=(2\overline{S}_{i,j}\overline{S}_{i,j})^{1/2}$ is its norm. Model coefficients $(C_s\Delta)^2$ and $(C_c\Delta)^2$ are computed following the dynamic procedure described by Lilly (1992) and implemented by Tejada-Martínez and Grosch (2007) and Tejada-Martínez *et al*. (2009).

Our simulation methodology consists of LES with well-resolved molecular sublayers. In order to ensure such resolution, the grid is sufficiently refined near the surface. Thus, the previously described SGS stress and SGS scalar flux are small compared to the resolved viscous stress and diffusive flux in the nearsurface region. Furthermore, the SGS models contribute less than 3 percent of the dissipation.

Finally, we note that the Craik-Leibovich vortex force in (1) is a purely inviscid mechanism, thus it does not directly affect molecular sublayers. This mechanism does generate Langmuir turbulence thereby altering the flow and ultimately the molecular sublayers. As described by Veron and Melville (2001) based on their laboratory experiments, it is the turbulence generated by the surface waves, and not the surface waves by themselves that dictates molecular sublayer behavior. This can also be concluded from the airborne infrared observations of Marmorino *et al*. (2005). Their imagery demonstrates that Langmuir cells induce a cooling of the ocean surface along the surface convergence zone of the cells. Consistent with these laboratory and field observations, our computational

approach focuses on capturing the main features associated with Langmuir turbulence via the Craik-Leibovich force (rather than through direct resolution of surface waves) in order to gain a better understanding of the impact of this turbulence regime on molecular sublayers.

3. Results and discussion

3.1 Computational setup

Equations (1)-(3) have been presented in dimensionless form for ease of definition of parameters such as Re and La_t. Henceforth, all LES flow variables will be considered dimensional unless specified otherwise.

Flow configurations considered in our LES studies are sketched in Figure 1. As noted earlier, wave-current interaction generating LC is represented through the Craik-Leibovich vortex force (Craik and Leibovich 1976), enabling LES to be performed with a rigid-lid (flat) top surface where zero normal flow is imposed. The domain depicted in Figure 1a is for pressure gradient-driven shear flow, typical of a tidal flow with small or zero surface wind stress. In wind-driven shear flow (depicted in Figure 1b) constant wind stress is prescribed at the top surface. In our wind-driven flows, wind stress is applied such that the Reynolds number is $Re=395$. The body force or pressure gradient in the flow depicted in Figure 1a is applied such that $Re=395$ as well. No-slip boundary condition is applied at the bottom walls. Furthermore, periodic boundary conditions are set in the horizontal (x_1 and x_2 or downwind and crosswind) directions. The domain size in the crosswind (x_2) direction is $(8/3)\pi\delta$, chosen to adequately resolve one Langmuir cell as measured during the field observations of Gargett *et al*. (2004) and Gargett and Wells (2007). Dirichlet boundary conditions for concentration are prescribed at the bottom ($x_3=-\delta$) and top ($x_3=\delta$) of the domains. Scalar concentration prescribed at the bottom is $C_{-\delta}$ and at the top is C_δ with $C_\delta > C_{-\delta}$. The latter interfacial condition is representative of the air side essentially serving as an infinite reservoir of the scalar with a constant concentration. In all simulations presented, the

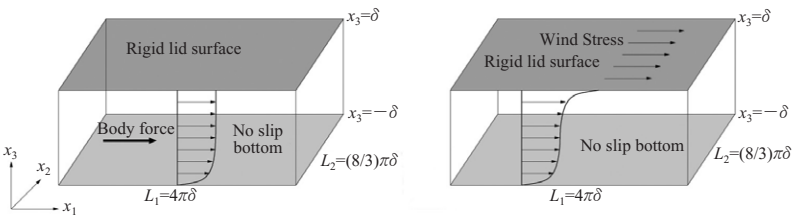

Figure 1 Flow configurations for pressure gradient-driven flow (a: left) and wind-driven flow (b: right). Domain lengths are given in dimensional form where δ is water column half-depth.

Schmidt number is set to $Sc=1$.

The governing equations in (1) within the previously described domain configurations were solved using the hybrid spectral/finite-difference solver of Tejada-Martínez and Grosch (2007) in which horizontal (x_1 and x_2) directions are discretized using fast Fourier transforms and the vertical (x_3) direction is discretized using 5th and 6th order compact finite-difference schemes. All simulations were performed on a grid with 32 modes in the downwind (x_1) direction, 64 modes in the crosswind (x_2) direction and 96 points in the vertical (x_3) direction. This grid is uniform in x_1 and x_2 and highly stretched in x_3 in order to resolve surface molecular sublayers. In all flows, the first grid point off the surface is at distance $x_3^+=1$, which is well within the surface molecular sublayers. Note that x_3^+ measures distance to the surface in wall units (i.e. $x_3^+=(\delta-x_3)u_\tau/\nu$).

3.2 Statistics

LES results under statistical equilibrium are shown for pressure gradientdriven flow without LC, wind-driven flow without LC and various wind-driven flows with LC. The flows with LC are characterized by different turbulent Langmuir numbers (La_t): 1.0, 0.7 and 0.4. As defined earlier, the square of the turbulent Langmuir number, La_t^2, is inversely proportional to the strength of wave forcing relative to wind forcing. Thus, decreasing the value of La_t serves to increase the turbulent intensity and coherency of the Langmuir cells, especially within the downwelling and upwelling limbs of the cells. In all cases, the dominant wavelength λ of surface waves was set to $\lambda=12\delta$. Parameters $La_t=0.7$ and $\lambda=12\delta$ are representative of the field observations of Gargett *et al*. (2004) and Gargett and Wells (2007). Note that in our LES, $Re=395$ is much lower than the $Re=$O (50000−100000) recorded in the field measurements of Gargett and collaborators, thereby making our LES a laboratory-scale LES. However, note that in our LES, $La_t=0.7$ as was recorded in the field. Thus, our LES is driven by the same wave forcing relative to wind forcing measured in the field. As described in the introduction, Tejada-Martínez and Grosch (2007) have shown that major characteristics of resolved full-depth LC in the winddriven flow with $La_t=0.7$ and $\lambda=12\delta$ are in general agreement with the field measurements of full-depth LC of Gargett and collaborators.

3.2.1 Mean turbulent quantities

Figure 2 shows mean concentration and mean downwind velocity in wall units. Mean downwind velocity in wall units is defined as $u^+=\langle\overline{u}_1\rangle/u_\tau$, where $\langle\cdot\rangle$ denotes averaging over horizontal directions and time. The action of LC serves to homogenize momentum and concentration throughout the water column inducing

thinner molecular sublayers at the surface. As discussed earlier, a smaller La_t corresponds to larger wave forcing and more intense LC. This is consistent with the results of Figure 2 showing that the degree of homogenization of concentration and momentum is highest in the flow with lowest La_t.

Transfer velocity, K, is defined proportional to the vertical gradient of mean concentration evaluated at the surface and is expressed as

$$K=\frac{D_c}{\Delta C}\left(\frac{d\langle\overline{C}\rangle}{dx_3}\right)_{x_3=\delta}. \tag{4}$$

where ΔC is the difference between scalar concentration at the surface (C_δ) and the bulk (Calmet and Magnaudet 1998). As the intensity of full-depth Langmuir cells increases, gas transfer velocity also increases. Furthermore, the wind-driven flow with LC and $La_t=0.7$ leads to a 60 percent increase in transfer velocity relative to the wind-driven flow without LC. This is partly due to an increase in the vertical gradient of mean concentration at the surface and partly due to a decrease in ΔC. Both of these effects can be seen in Figure (2a). Such a dramatic increase in K but in the presence of small-scale LC has been reported by Veron and Melville (2001) based on laboratory experiments. Further below we will test the accuracy of

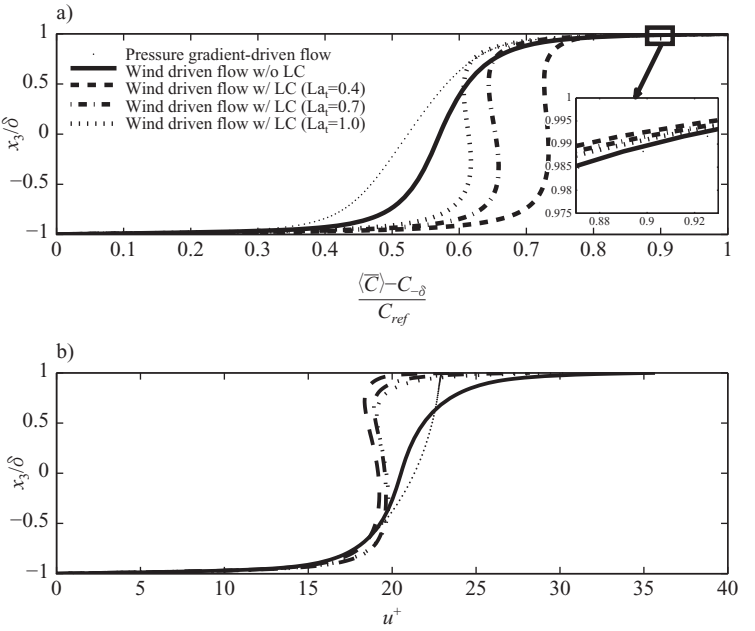

Figure 2 Near-surface mean concentration (a) and mean downwind velocity in wall units (b). Note that mean downwind velocity in wall units is defined as $u^+=\langle\overline{u}_1\rangle/u_\tau$. C_{ref} is concentration at the top (C_δ) minus concentration at the bottom ($C_{-\delta}$).

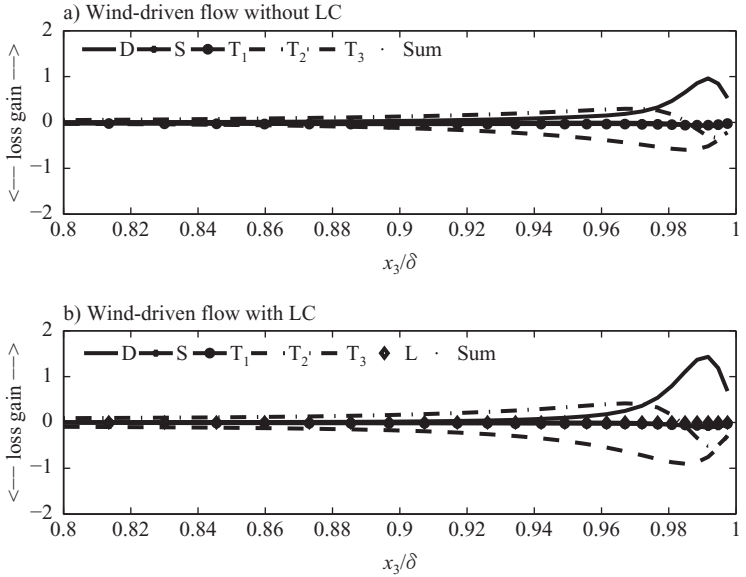

Figure 3 Near-surface budgets of Reynolds-averaged scalar transport equation in wind-driven flow without LC and in wind-driven flow with LC (with $La_t=0.7$). Note that summation of the budget terms is zero under statistical equilibrium.

several parameterizations of K in predicting these trends associated with LC.

3.2.2 Near-surface transport

We perform statistical analysis of turbulent quantities in order to elucidate nearsurface turbulent transport in our wind-driven flows. Figure 3 shows budgets of the Reynolds-averaged scalar transport equation under statistical equilibrium for wind-driven flows with LC (with $La_t=0.7$) and without LC:

$$\underbrace{-\frac{1}{La_t^2}\phi_j^s\frac{d\langle\overline{C}\rangle}{dx_3}}_{L}+\underbrace{-\frac{1}{ReSc}\frac{d^2\langle\overline{C}\rangle}{dx_3^2}}_{D}+\underbrace{\frac{d\langle q_3\rangle}{dx_3}}_{S}\underbrace{-\left\langle u_1'\frac{\partial\overline{C}'}{\partial x_1}\right\rangle}_{T_1}\underbrace{-\left\langle u_2'\frac{\partial\overline{C}'}{\partial x_2}\right\rangle}_{T_2}\underbrace{-\left\langle u_3'\frac{\partial\overline{C}'}{\partial x_3}\right\rangle}_{T_3}=0 \qquad (5)$$

where L is Craik-Leibovich vortex (Langmuir) forcing, D is molecular diffusion, S is the subgrid-scale flux and T_1, T_2 and T_3 are transports in downwind, crosswind and vertical directions, respectively. Note that all of the previous terms are given in dimensionless form. Near the surface, in wind-driven flows with and without LC, dominant terms are molecular diffusion, crosswind transport and vertical

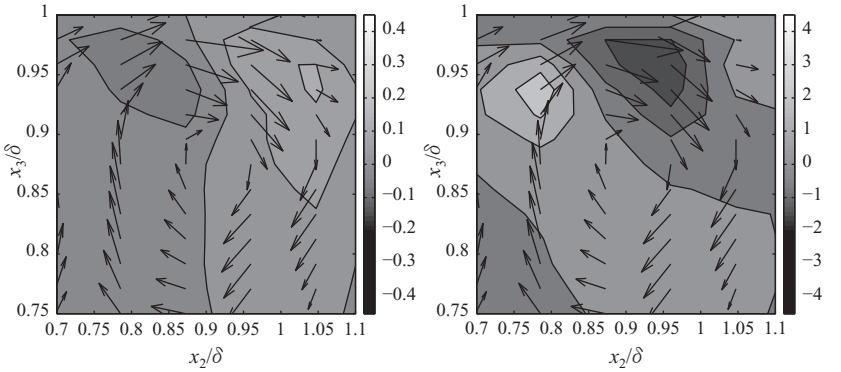

Figure 4 Conditionally averaged velocity fluctuation vectors superimposed with color contour of (a) conditionally averaged concentration fluctuation $\langle \overline{C}' \rangle_{conditional}$ and (b) conditionally averaged crosswind transport defined as $T_2 = -\langle u_2' \partial \overline{C}' / \partial x_2 \rangle_{conditional}$ in wind-driven flow without LC. Conditional averaging is performed over the downwind direction and time similar to that described by Debusschere and Rutland (2004). Note that the structures in this figure are of small scale appearing within the uppermost one-eighth of the water column.

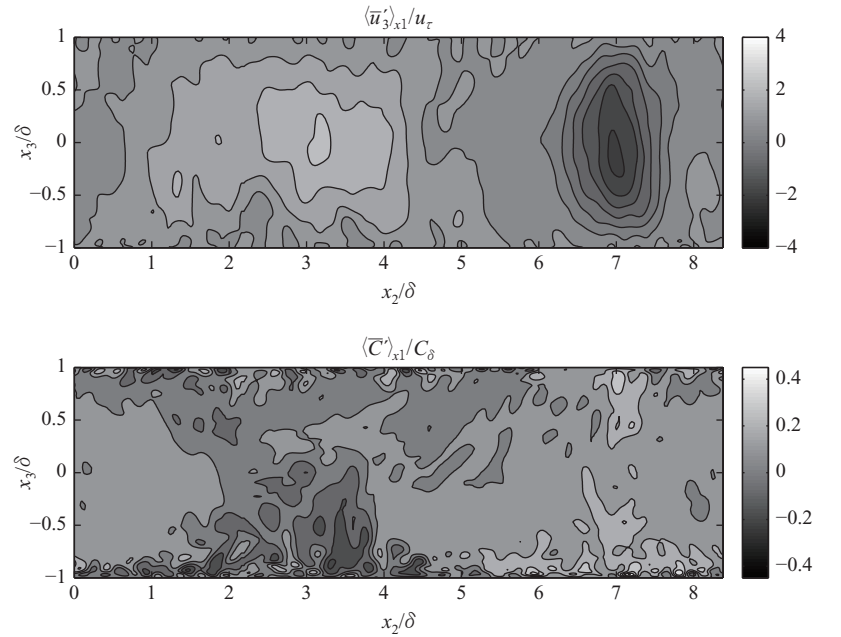

Figure 5 Instantaneous vertical velocity fluctuations (top) and concentration fluctuations (bottom) averaged over the downwind (x_1) direction in wind-driven flow with LC ($La_t = 0.7$). Downwelling limb of full-depth LC (characterized by a full-depth region of negative vertical velocity fluctuations) coincides with a full-depth region of positive concentration fluctuations and vice-versa.

transport. In wind-driven flow with LC, near-surface peaks of these dominant terms are approximately 50 percent higher than in the flow without LC. Thus, the near-surface effect of LC is to enhance diffusion and crosswind and vertical turbulent transports of the scalar. Note that the nearsurface contribution of the Langmuir forcing term in the Reynolds-averaged scalar transport equation in (5) is negligible. We conclude that the contribution of LC on scalar transport is not through Langmuir forcing directly, but rather through the strongly coherent large-scale turbulent structures associated with LC greatly affecting diffusion and turbulent transport of the scalar.

In the wind-driven flow without LC, near-surface crosswind transport is found to be strongly correlated with small eddies. Figure 4 shows conditionally averaged velocity vectors in the upper-most one-eighth region of the water column (between $x_3/\delta=0.75$ and $x_3/\delta=1$) in wind-driven flow without LC. These vectors reveal the presence of a near-surface, clockwise-rotating small eddy strongly correlated with concentration fluctuation $\overline{C}'$, as shown in Figure 4a. The downward moving, right side of the eddy takes high concentration fluid from the surface to depths below, while the upward moving, left side of the eddy takes low concentration fluid from below up to the surface. This transport induces a region characterized by a surface

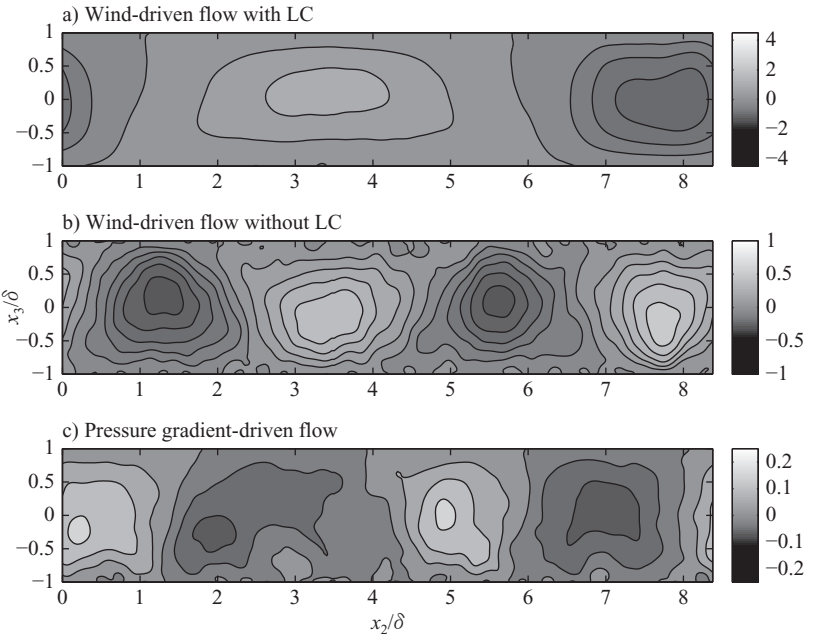

Figure 6 Vertical velocity fluctuations, $\overline{u_3'}/u_\tau$, averaged over the downwind (x_1) direction and over time for different flows. In wind-driven flow with LC, $La_t=0.7$. Note the difference in velocity fluctuation magnitudes between the different flows.

positive crosswind gradient of $\overline{C}'$ (Figure 4a) which together with the positive crosswind velocity fluctuations ($\overline{u_2}'$) induced by the eddy at the surface lead to the surface region of negative crosswind transport, T_2, seen in Figure 4b.

In the wind-driven flow with full-depth LC, we have found that near-surface eddies of the size of the eddy in Figure 4 are not present, having been diminished by large-scale eddies (i.e. full-depth LC). As can be seen in Figure 5, the fulldepth downwelling limb of the LC coincides with a full-depth region of positive concentration fluctuations, consistent with the transport of high concentration fluid from the surface to the bottom. Thus, full-depth LC dominates scalar transport near the surface as well as everywhere else in the water column.

3.3 Evaluation of transfer velocity models

As noted earlier, LES with molecular sublayer resolution allows for the comparison of transfer velocity predicted by parameterizations (models) with transfer velocity obtained directly in the LES via equation (4). In surface renewal theory, transfer velocity is computed as $K=(D_c/\tau)^{1/2}$ where τ is the surface renewal time scale. The surface renewal time scale is computed based on dominant hydrodynamic processes influencing near-surface scalar transport, as described in the introduction.

Gulliver and Halverson (1989) showed that in a laboratory flume, surface renewal is dominated by the full-depth upwellings of streamwise vortices associated with secondary currents of Prandtls second kind typically found in such flumes. Based on this, they proposed a large eddy model of the surface renewal time scale computed as $\tau \propto 1/(w_s/h)F_r$ where w_s is the maximum vertical velocity associated with the streamwise vortices, F_r is the fraction of an eddy consisting of an upwelling and h is the depth of the water column. It will be shown further below that this model is successful for wind-driven flows with full-depth LC, as expected from our earlier results showing that full-depth LC profoundly influences scalar transport near the surface and everywhere else in the water column.

In order to evaluate parameter F_r in the large eddy model, we collected vertical velocity fluctuations averaged over the downwind direction and time in all of our flows (Figure 6). In this figure it can be seen that the upwelling and downwelling limbs of full-depth LC (with $La_t=0.7$) are strongly coherent in the downwind direction. Wind-driven flow without LC and pressure gradientdriven flow are also characterized by downwind-coherent, large-scale (full-depth) upwellings and downwellings. However, these structures are not as coherent as full-depth LC, reflected by the lower magnitudes of partially averaged vertical velocity fluctuations in the flows without LC in Figures 6b,c. In wind-driven flow without LC, the full-depth structures are referred to as Couette cells (see Tejada-Martínez

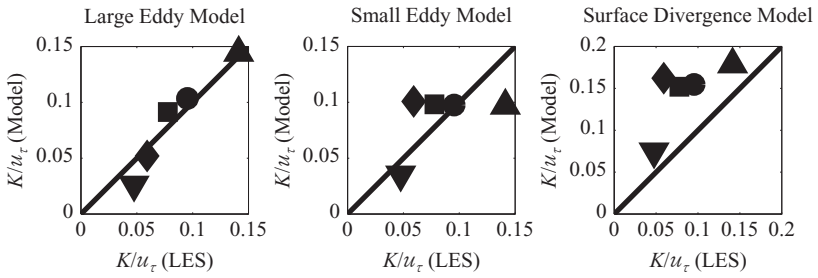

Figure 7 Comparison of transfer velocity predicted by various parameterizations (models) versus transfer velocity obtained directly in the LES. Each symbol corresponds to a particular flow. Triangles: wind-driven flow with LC and $La_t=0.4$; Circles: wind-driven flow with LC and $La_t=0.7$; Squares: wind-driven flow with LC and $La_t=1$; Diamonds: wind-driven without LC; Triangles upside-down: pressure gradient-driven flow.

and Grosch (2007) for further details).

Finally, performing a depth average of the upwelling limbs in Figure 6 leads to $F_r=0.60$ for the wind-driven flow with LC and $La_t=0.7$, $F_r=0.5$ for the wind-driven flow without LC and $F_r=0.42$ for the pressure gradient-driven flow. Although not shown here, it was also found that $F_r=0.46$ and $F_r=0.63$ for wind-driven flows with LC with $La_t=0.4$ and $La_t=1$, respectively.

In addition to the large eddy model, we will evaluate two other parameterizations of transfer velocity. In the small eddy model (Banerjee *et al*. 1968; Lamont and Scott, 1970; Zappa *et al*. 2007) surface renewal time scale is taken to be $\tau \propto (\nu/\varepsilon)^{1/2}$, where ε is dissipation rate of turbulent kinetic energy evaluated at the surface (see Calmet and Magnaudet (1998) for details regarding model coefficients). According to this model, an increase in ε at the surface gives rise to an increase in transfer velocity.

In the surface divergence model (McCready, 1986; Banerjee *et al*. 2004) $\tau \propto \langle \beta^2 \rangle^{-1/2}$, where $\beta = -\partial u_3'/\partial x_3$ evaluated at the surface (see McCready (1986) for details regarding model coefficients). Note that β is a signature of surface divergence and surface renewal caused by small-scale turbulence events often referred to as "sweeps" (Banerjee *et al*. 2004). According to this model, increasing the magnitude of surface divergence gives rise to an increase in transfer velocity.

As previously described and illustrated by the results of Figure 6, partially averaged vertical velocity fluctuations (averaged over x_1 and time) reveal the strength or coherency of the downwind-elongated, large-scale (full-depth) structures present in all of our flows. The flow with weakest large structures is the pressure gradient-driven flow followed by the wind-driven flow without LC. In flows with LC, the strength of the large structures (i.e. the strength of the fulldepth LC) increases with decreasing turbulent Langmuir number, La_t. Figure 7 shows

transfer velocity, K, predicted by the models (parameterizations) described earlier versus K obtained directly in the LES via equation (4). The LES predicts an increasing transfer velocity with increasing strength of large-scale structures. For example in wind-driven flow with LC (with $La_t = 0.7$), transfer velocity is 60 percent higher relative to wind-driven flow without LC. Figure 7 shows that the large eddy model performs best, being able to predict a similar increasing trend in transfer velocity. Meanwhile, the small eddy model and the surface divergence model are not able to predict this increase and actually predict a smaller transfer velocity in wind-driven flow with LC (with $La_t = 0.7$) than in wind-driven flow without LC. In the case of the small eddy model, the reason for this is that turbulent kinetic energy dissipation rate (ε) at the surface in the flow with LC (and $La_t = 0.7$) is slightly smaller than in the wind-driven flow without LC; recall that in this model an increase in ε at the surface gives rise to an increase in transfer velocity. Overall, there is no significant difference between the wind-driven flows in terms of ε at the surface.

The reason the surface divergence model fails to predict the greater transfer velocity in the wind-driven flow with LC (with $La_t = 0.7$) compared to its counterpart without LC is because the magnitude of surface divergence in the latter is actually greater than in the former; recall that in this model increasing surface divergence magnitude gives rise to an increase in transfer velocity. In wind-driven flows with LC, an increasing trend of surface divergence magnitude is seen with decreasing La_t, thus the surface divergence model is able to correctly predict an increasing trend in transfer velocity with a decrease in La_t.

We finally note that the small eddy model and the surface divergence model perform well for the flow with weakest large-scale structures (i.e. the pressure gradient-driven flow). The large eddy model performs well for all the flows considered.

4. Conclusions

Statistical analysis of LES results showed that full-depth LC dominates near-surface mass transport as well as transport throughout the entire water column in wind-driven shear flow with a no-slip bottom. In the absence of LC, near-surface small eddies contribute towards the mass transport at the air-water interface. These small eddies are diminished in the presence of LC. The surface transfer velocity predicted by the large eddy model of Gulliver and Halverson (1989) based on surface renewal time scale given by characteristics of large streamwise vortices was found to be well-correlated with transfer velocity predicted by the LES. Furthermore, an increasing trend of LES-computed surface transfer velocity with increasing surface divergence magnitude was observed for sufficiently coherent

large-scale structures, but not necessarily for the weakest of these structures. Finally, dissipation rate of turbulent kinetic energy at the surface in LES of flows with LC did not correlate with transfer velocity evaluated directly in the LES.

In the present study, the surface (the air-water interface) has been taken to be flat. However, during occurrences of full-depth LC under moderate wind conditions the surface is expected to be characterized by capillary ripples and microbreaking waves. Several theories have been developed to account for the role of capillary ripples on surface mass transfer (e.g. see Csanady, 1990). These developments together with our results showing the impact of full-depth LC on surface renewal suggest further research in order to determine the combined effect of full-depth LC and the small-scale turbulent structure associated with capillary ripples on mass transfer at the surface.

In our simulations we have set $Re=395$ and $Sc=1$ much lower than in natural conditions in order to be able to resolve molecular sublayers. In the field measurements of full-depth LC of Gargett *et al*. (2004) and Gargett and Wells (2007), $Re=O(50000-100000)$. Furthermore, under natural conditions, $Sc=200$ for a dissolved gas in water such as CO_2 in water, thus the thickness of the diffusive sublayer is much less than the thickness of the viscous sublayer. The current simulations are an initial attempt at understanding the impact of fulldepth Langmuir circulation (LC) on near-surface turbulent scalar transport and we are in the process of extending our simulations to higher Schmidt numbers in order to understand the Schmidt number dependence of scalar transport at the surface and gas transfer velocity in the presence of full-depth LC.

5. Sponsors

These studies were supported through a U.S. National Science Foundation CAREER Award (CBET-0846510) made to A.E. Tejada-Martínez. The authors would also like to acknowledge the use of the services provided by Research Computing, University of South Florida.

References

Banerjee, S., D. Scott and E. Rhodes (1968), Mass transfer to falling wavy liquid films in turbulent flow (Journal), *Ind. Eng. Chem. Fundamentals*, 22-27.

Banerjee, S., D. Lakehal and M. Fulgosi (2004), Surface divergence models for scalar exchange between turbulent streams (Journal), *Int. J. Multiphase Flow, 30*, 963-977.

Calmet, I. and J. Magnaudet (1998), High-Schmidt number mass transfer through turbulent gas-liquid interfaces (Journal), *Int. J. Heat Fluid Flow, 19*, 522-532.

Craik, A. D. D. and S. Leibovich (1976), A rational model for Langmuir Circulation (Journal), *J. Fluid Mech., 73*, 401-426.

Csanady, G. T. (1990), The role of breaking wavelets in air-sea gas transfer (Journal), *J.*

Geophys. Res., 95, 749-759.

Debusschere, B. and C. Rutland (2004), Turbulent scalar transport mechanisms in plane channel and Couette flows (Journal), *Int. J. Heat Mass Transfer, 47*, 1771-1781.

Donelan, M.A. and R. Wanninkhof (2002), *Gas Transfer at Water Surfaces - Concepts and Issues, Chapter in Gas Transfer at Water Surfaces (Book)*, Geophysical Monograph # 127, American Geophysical Union, 1-10.

Gargett, A., J. Wells, A.E. Tejada-Martínez, and C.E. Grosch, (2004), Langmuir supercells: a mechanism for sediment resuspension and transport in shallow seas (Journal), *Science*, 306, 1925-1928.

Gargett, A. E., and J. R. Wells (2007), Langmuir turbulence in shallow water: Part I. Observations (Journal), *J. Fluid Mech., 576*, 27-61.

Gulliver, J. S. and M. J. Halverson, (1989), Air-water gas transfer in open channels (Journal), *Water Resources Res., 25*, 1783-1793.

Lamont, J. C. and D. S. Scott (1970), An eddy cell model of mass transfer into the surface of a turbulent liquid (Journal), *AIChE J., 16(4)*, 513-519.

Langmuir, I. (1938), Surface motion of water induced by wind (Journal), *Science, 87*, 119-123.

Lilly, D. K. (1992), A proposed modification of the Germano subgrid-scale closure (Journal), *Phys. Fluids, 3*, 2746-2757.

Liu, W. and J. Businger (1975), Temperature profile in the molecular sublayer near the interface of fluid in turbulent motion (Journal), *Geophys. Res. Lett., 2*, 403-404.

Marmorino, G. O., G. B. Smith and G. J. Lindemann (2005), Infrared imagery of large-aspectratio Langmuir circulation (Journal), *Cont. Shelf Res., 25*, 1-6.

McCready, M., E. Vassiliadou and T. Hanratty, Computer simulation of turbulent mass transfer at a mobile interface (Journal), *AIChE J., 32(7)*, 1108-1115.

McWilliams, J. C., P.P. Sullivan and C.-H Moeng (1997), Langmuir turbulence in the ocean (Journal), *J. Fluid Mech., 334*, 1-30.

Phillips, O. M. (1967), Dynamics of the Upper Ocean (BooK), Cambridge Univ. Press.

Soloviev, A. and P. Schlüessel (1994), Parameterization of the cool skin of the ocean and of the air-ocean gas transfer on the basis of modeling surface renewal (Journal), *J. Phys. Oceanogr., 24(1339-1346)*, 1339-1346.

Tejada-Martínez, A.E. and C.E. Grosch (2007), Langmuir turbulence in shallow water: Part 2. Large-eddy simulation (Journal), *J. Fluid Mech., 576*, 63-108.

Tejada-Martínez, A. E., C. E. Grosch, A. E. Gargett, J. A. Polton, J. A. Smith, and J. A. MacKinnon (2009), A hybrid spectral/finite-difference large-eddy simulator of turbulent processes in the upper ocean (Journal), *Ocean Model., 30*, 115-142.

Thorpe, S.A. (2004), Langmuir circulation (Journal), *Annu. Rev. Fluid Mech., 36*, 55-79.

Veron, F. and W. K. Melville (2001), Experiments on the stability and transition of wind-driven water surface (Journal), *J. Fluid Mech., 446*, 22-65.

Zappa, C.,W. McGillis, P. A. Raymond, J. B. Edson, E. J. Hintsa, H. J. Zemmelink, J.W. Dacy, and D. T. Ho (2007), Environmental turbulent mixing controls on air-water gas exchange in marine and aquatic systems (Journal), *Geophys. Res. Lett., 34*, L10601.